The Pathogenic Human Sulfite Oxidase Mutants G473D and A208D Are Defective in Intramolecular Electron Transfer†

Changjian Feng,‡ Heather L. Wilson,§ Gordon Tollin,*,|| Andrei V. Astashkin,‡ James T. Hazzard,|| K. V. Rajagopalan,*,§ and John H. Enemark*,‡

Department of Chemistry, University of Arizona, Tucson, Arizona 85721, Department of Biochemistry, Duke University Medical Center, Durham, North Carolina 27710, and Department of Biochemistry and Molecular Biophysics, University of Arizona, Tucson, Arizona 85721

Received May 16, 2005; Revised Manuscript Received August 12, 2005

ABSTRACT: Mutations G473D and A208D were identified in patients with isolated sulfite oxidase (SO) deficiency, and the equivalent amino acids (G451 and A186, respectively) have been localized to the vicinity of the molybdopterin active site in the X-ray structure of chicken SO [Kisker, C., Schindelin, H., Pacheco, A., Wehbi, W., Garrett, R. M., Rajagopalan, K. V., Enemark, J. H., and Rees, D. C. (1997) *Cell 91*, 973−983]. To assess the effects of these mutations in human SO, steady-state kinetic studies of enzyme turnover and laser flash photolysis measurements of intramolecular electron transfer (IET) rate constants between the reduced heme [Fe(II)] and Mo(VI) centers were carried out in the recombinant G473D, G473A, G473W, G473D/R212A, and A208D human SO mutants. In the G473D and A208D mutants, the IET rate constants at pH 6.0 are decreased by 3 orders of magnitude relative to that of the wild type. Steady-state kinetic measurements indicate that the IET process is the rate-limiting step in the catalytic cycle of these two mutants. Thus, the large decreases in the IET rate constants and the k_{cat} values, and the large increases in the $K_m^{sulfite}$ values, rationalize the fatal impact of these mutations. Far-UV CD spectra of G473D indicate that the protein backbone conformation is remarkably changed, and the sedimentation equilibrium indicates that the protein is monomeric. Furthermore, EPR studies also suggest that the active site structure of the Mo(V) form of A208D is different from that of the wild type. In contrast, similar studies on G473A show that it is dimeric, that its Mo(V) active site structure is similar to that of the wild type, and that its IET rate constant is only 2.6-fold smaller than that of the wild type. IET in G473W is severely impaired, and no IET is observed for G473D/R212A. In chicken SO, the equivalent residues (G451 and A186) are both buried inside the protein. Thus, for human SO, the mutations to charged residues at the equivalent sites most likely cause crucial global or localized structural changes, and expose an alternative docking site that may compete with the Mo domain for docking of the heme, thereby retarding IET and efficient catalytic turnover of the sulfite oxidation reaction.

In animals, the molybdenum-containing enzyme sulfite oxidase (SO,[1] EC 1.8.3.1) catalyzes the oxidation of sulfite to sulfate, with ferricytochrome *c* [(cyt *c*)$_{ox}$] as the physiological electron acceptor (*1*−*5*):

$$SO_3^{2-} + H_2O + 2(\text{cyt } c)_{ox} \rightarrow SO_4^{2-} + 2(\text{cyt } c)_{red} + 2H^+ \quad (1)$$

This is the final step in the oxidative degradation of the sulfur-containing amino acids cysteine and methionine, and is physiologically essential. The enzyme also plays an important role in detoxifying exogenously supplied sulfite and sulfur dioxide. The enzymes of the SO superfamily consist of SO from animals (*6*) and plants (*7*), bacterial sulfite dehydrogenase (SDH) (*8*), and the assimilatory nitrate reductase from eukaryotes (*9*).

Sulfite oxidase deficiency is an inherited metabolic disorder in humans that results in profound birth defects, severe neonatal neurological problems, and early death, with no effective therapies known (*10*, *11*). The inborn error is characterized by dislocation of ocular lenses, mental retardation, and, in severe cases, attenuated growth of the brain (*12*). The biochemical basis of the pathology of sulfite oxidase deficiency is not yet known. Fatal brain damage may be due to the accumulation of a toxic metabolite (possibly SO_3^{2-},

† This work was supported by Grants GM 37773 to J.H.E., DK 15057 to G.T., and GM 44283 to K.V.R. from the National Institutes of Health.

* To whom correspondence should be addressed. J.H.E.: e-mail, jenemark@u.arizona.edu; phone, (520) 621-2245; fax, (520) 626-8065. G.T.: e-mail, gtollin@u.arizona.edu; fax, (520) 621-9288. K.V.R.: fax, (919) 684-8919; e-mail, raj@biochem.duke.edu.

‡ Department of Chemistry, University of Arizona.

§ Duke University Medical Center.

|| Department of Biochemistry and Molecular Biophysics, University of Arizona.

[1] Abbreviations: Mo, molybdenum; SO, sulfite oxidase; SDH, sulfite dehydrogenases; (cyt *c*)$_{ox}$ and (cyt *c*)$_{red}$, ferricytochrome *c* and ferrocytochrome *c*, respectively; IET, intramolecular electron transfer; k_{et}, rate constant for IET; EPR, electron paramagnetic resonance; CW, continuous wave; CD, circular dichroism; wt, wild type; dRF and dRFH•, 5-deazariboflavin and 5-deazariboflavin semiquinone, respectively; Tris, tris(hydroxymethyl)aminomethane; Bis-Tris, bis(2-hydroxyethyl)aminotris(hydroxymethyl)methane; Pipes, 1,4-piperazinediethanesulfonic acid; Bicine, *N*,*N*-bis(2-hydroxyethyl)glycine.

10.1021/bi050907f CCC: $30.25
Published on Web 09/29/2005

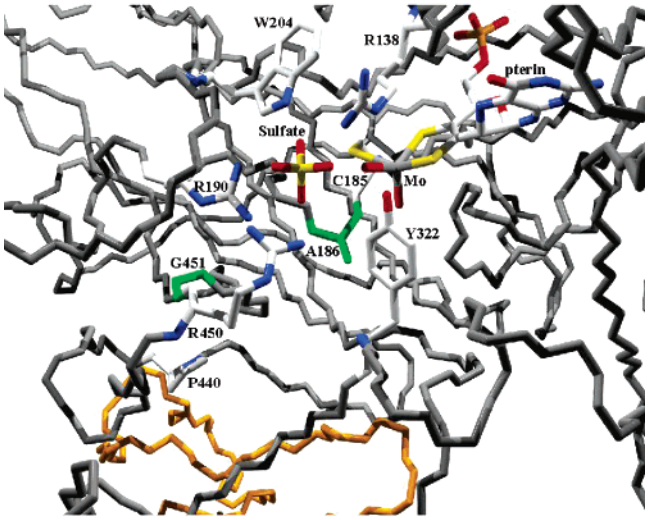

FIGURE 1: Selected amino acids, ligands, and part of the polypeptide chain in chicken SO. One subunit is colored black, and part of the dimerization domain of another subunit is colored yellow. The selected amino acids and/or ligands are colored by CPK, except for G451 and A186 which are colored green. G451 and A186 in chicken SO are the equivalents of G473 and A208 in human SO, respectively. Note that G451 and A186 are buried underneath the protein surface. Coordinates for this figure were from the Protein Data Bank (PDB entry 1SOX). This figure was generated with Deep View version 3.7 (http://www.expasy.org/spdbv/) and rendered with POV-Ray version 3.5 (http://www.povray.org).

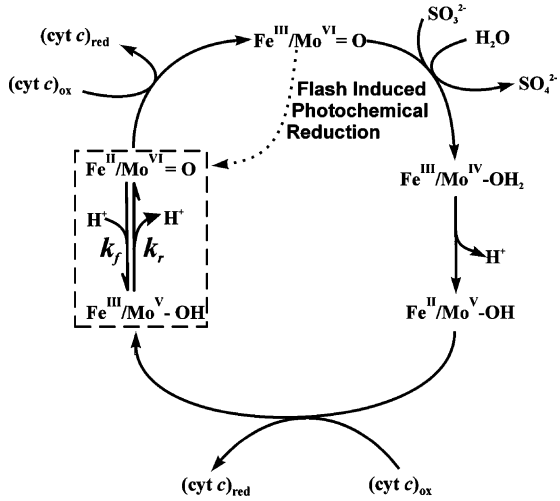

FIGURE 2: Proposed oxidation-state changes occurring at the Mo and Fe centers of native animal SO during the catalytic oxidation of sulfite and the concomitant reduction of (cyt c)$_{ox}$. Only the equatorial oxygen atom among the ligands of Mo is shown for clarity. Note that intermediate Fe^{II}/Mo^{V}-OH in the reductive half-reaction can be detected by EPR. The one-electron reduction of Fe^{III} indicated by a dotted arrow connecting $Mo^{VI}Fe^{III}$ and Mo^{VI}-Fe^{II} can be initiated with a laser pulse in a solution containing dRF and the sacrificial electron donor semicarbazide. The subsequent IET between $Mo^{VI}Fe^{II}$ and $Mo^{V}Fe^{III}$, which is of interest in this study, is highlighted in the dashed box. The rate constants of forward and reverse IET (k_f and k_r, respectively) are defined in the text.

which is a strong nucleophile that can react with a wide variety of cell components); alternatively, a deficiency in the reaction product (SO_4^{2-}) may disturb normal fetal and neonatal development of the brain (*2*, *3*). These severe neurological symptoms result from either point mutations in the SO protein itself (so-called isolated sulfite oxidase deficiency, in which only SO activity is affected) or the inability to properly produce the pyranopterindithiolate cofactor, which results in deficiencies in all Mo-containing enzymes (so-called Mo cofactor deficiency) (*2*, *13*, *14*). So far, several point mutations in human SO have been identified in patients suffering from isolated sulfite oxidase deficiency (*15*−*19*). These include G473D and A208D (*20*), which are of significant interest in this study. G473 and A208 in human SO are conserved in all SO species sequenced to date. The equivalent amino acids in chicken SO, for which a crystal structure is known (*20*), are G451 and A186, respectively.

The X-ray structure of native chicken SO has established the relationship of the heme and Mo domains (*20*). Each subunit of the homodimeric protein contains a small N-terminal b_5-type cytochrome domain, a large central Mo-binding domain, and a large C-terminal interface domain. In each subunit, the Mo domain and the b_5-type heme domain are linked by a flexible peptide loop of 10 amino acids. The molybdenum atom is coordinated by five ligands with approximate square pyramidal coordination geometry (Figure 1). The terminal oxo group occupies the axial position, and the equatorial positions are occupied by three sulfur atoms (one from C185 and two from pterin) and one water/hydroxo ligand. The equatorial Mo^{V}-OH group can be directly detected by continuous wave (CW) and pulsed electron paramagnetic resonance (EPR) spectroscopy (see below). As expected for binding an anionic substrate, the sulfite binding site is highly positively charged, and consists of three arginines (R138, R190, and R450), W204, and Y322. A186 is ~3.8 Å from the Mo atom, and is close to Y322. A186 is also near a hydrophobic pocket that is formed by I342, L345, V452, and L453. G451 is more distant (~12 Å) from the Mo center, and adopts unique torsion angles ($\varphi = 62°$, $\psi = 32°$) that are normally observed in left-handed α-helices. G451 is not part of the region immediately surrounding the sulfite binding domain. It is located on what could be considered the "back face" of the protein below R190 and R450 in Figure 1. Note that G451 is close to the C-terminal dimerization domain, which has a fold that provides the principal contacts between the two subunits of the protein (Figure 1). Importantly, both A186 and G451 are buried inside the protein with very little solvent accessibility.

In the generally accepted mechanism for native SO in animals (Figure 2) (*21*, *22*), sulfite is oxidized to sulfate at the Mo center, and the reducing equivalents are passed on to the b_5 heme, where, in turn, the terminal electron carrier (cyt c)$_{ox}$ is reduced. The reductive half-reaction starts with the reaction of the Mo(VI) center in the fully oxidized SO with sulfite to produce sulfate. The transient two-electron reduced form of Mo(IV)/Fe(III) undergoes intramolecular electron transfer (IET) to generate the Mo(V)/Fe(II) form that can be detected by EPR spectroscopy (Figure 2) (*23*−*27*). In the oxidative half-reaction, a one-electron transfer to exogenous (cyt c)$_{ox}$ accomplishes reoxidation of the Fe(II) center, and leaves the enzyme in the one-electron reduced form of Mo(V)/Fe(III). A second Mo → Fe IET step [giving Mo(VI)/Fe(II)], followed by reduction of a second equivalent of (cyt c)$_{ox}$, regenerates the enzyme to the fully oxidized state of Mo(VI)/Fe(III). Recent attempts to mimic the physiological electron acceptor cyt c by a modified electrode are gaining more interest for the development of novel sulfite biosensors (*28*).

As a multi-redox-center enzyme, IET between the Mo and Fe centers in animal SO is fundamental to the function of the enzyme. We have previously shown that exogenous deazariboflavin radicals generated in situ with a laser pulse will rapidly reduce the Fe(III) center of SO by one electron (see the dotted arrow in Figure 2), followed by intramolecular equilibration between the redox centers. Note that this latter process corresponds to the second physiologically essential IET step highlighted in the dashed box in Figure 2, and the laser flash photolysis technique follows the IET process in the reverse direction of the enzymatic turnover. Comprehensive flash photolysis studies on native chicken SO and wild-type recombinant human SO have shown that the first-order IET rate constants between the reduced Fe(II) and oxidized Mo(VI) centers depend on the experimental conditions: solution viscosity (*29*, *30*), sulfate concentrations (*30*−*32*), and pH (*30*, *31*, *33*). The substantial viscosity dependence of IET, as well as constraints imposed by the large Fe···Mo distance (*34*), strongly suggests that in solution chicken SO may adopt a conformation that is an alternative to that seen in the crystal structure (*29*). This would most likely be driven by electrostatic interactions between the Mo and heme domains (*35*), thereby facilitating rapid IET by having an Fe···Mo distance much shorter than that observed in the X-ray structure. Very recently, electrochemical studies have also indicated that the motion of the heme domain is a controlling factor for chicken SO activity (*36*), and the conformational flexibility of chicken SO has been further supported by a recent pulsed electron−electron double-resonance spectroscopy study (*37*). Taken together, these results indicate that efficient IET between Mo(VI) and Fe(II) centers demands subtle and precise orientation of the two redox partners with respect to each other, and that the consequent IET-productive conformations of animal SO are vital to the facilitation of rapid IET between the two metal centers. Interestingly, a comparison of the crystal structures of chicken SO and *Arabidopsis thaliana* SO reveals possible surface regions in chicken SO for docking of its heme domain to the Mo domain in the course of IET and catalysis (*38*). SO is one of many biological electron transfer systems for which specific protein conformations are required for optimal function (*39*−*44*).

Heterodimeric bacterial SDH contains heme and Mo centers in separate tightly associated subunits, and thus, this enzyme represents a distinctly different type of sulfite-oxidizing enzyme (*45*), in which a fairly rigid positioning of the redox centers relative to one another is essential for maintaining the enzyme's integrity (*8*). In contrast to those for animal SO, the IET rate constants in SDH are not affected by either solution viscosity or the presence of the sulfate anion, indicating that IET in SDH proceeds directly within the protein medium and does not involve substantial motion of the two redox centers relative to each other (*46*). These results also provide direct evidence that the effects of sulfate anion and solution viscosity on IET in animal SO are due to interference with interdomain docking, and clearly demonstrate the differences between animal SO and bacterial SDH in terms of conformational gating effects.

Human (*47*−*49*) and rat (*50*) SO have been successfully cloned and expressed in highly active forms in *Escherichia coli*. Due to the lack of an X-ray structure for SO from either of these two species, the crystal structure of the highly homologous chicken SO provides a starting point and molecular basis for understanding the kinetic and spectroscopic studies of the effects of point mutations on recombinant human SO. It has been demonstrated that the combination of powerful rapid kinetic methods, such as flash photolysis, with site-directed mutagenesis can lead to the critical exploration of the involvement of specific amino acid residues in pathological human SO deficiencies. Thus, recent flash photolysis studies on IET in the Y343F (*30*) and R160Q (*35*) human SO mutants have provided direct evidence of the vital roles of Y343 and R160 in an efficient IET process. Very recent comprehensive stopped-flow analyses of the reductive half-reaction of Y343F and wild-type human SO along with the proteins lacking the N-terminal heme domain have clearly demonstrated that the Y343 residue is important for both substrate binding and oxidation of sulfite by human SO (*51*).

To better understand the mechanism for the lethal nature of the G473D and A208D mutations in infants, we have explored the role of the conserved G473 and A208 residues in human SO (the equivalent of G451 and A186 in chicken SO, respectively) in IET by comparative flash photolysis studies of the wild-type, G473D, G473A, G473W, G473D/R212A, and A208D human SO forms. The double mutant G473D/R212A was created to relieve possible steric interference between Asp 473 and Arg 212. The results clearly implicate the importance of G473 and A208 in controlling the rates of the IET process in human SO and allow the deleterious impact of these mutations to be rationalized.

EXPERIMENTAL PROCEDURES

Site-Directed Mutagenesis. The G473D and A208D mutations were identified and isolated from the cDNA of human patients with sulfite oxidase deficiency as previously described (*19*, *20*). These two patient-derived mutations were introduced into the pTG918 expression vector containing wild-type human SO (*48*) by subcloning from the pRG118 vector the fragment of the gene that contained the mutation (*19*). The G473A, G473W, and G473D/R212A mutations were directly introduced into pTG918 using the Transformer site-directed mutagenesis kit (Clontech) after appropriate mutagenic primers had been designed. All constructs were verified by sequence analysis performed at the Duke University DNA Analysis facility.

Expression and Purification of Wild-Type and Variant Human SO Proteins. Both recombinant wild-type and variant human SO proteins were expressed in the TP1000 strain of *E. coli* and purified as previously described (*48*) with the following modifications. After the phenyl-Sepharose column, fractions exhibiting an A_{414}/A_{280} ratio of ≥ 0.90 were further purified using a Superdex 200 FPLC column (Amersham Pharmacia) in 50 mM KPO_4 buffer containing 0.1 mM EDTA at pH 7.80. Fractions exhibiting an A_{414}/A_{280} ratio of ≥ 0.98 were then pooled and used in the experiments described in this study. The Mo content of purified SO proteins was determined using a Varian SpectrAA-220 double-beam atomic absorption spectrometer, and sample preparation was as previously described (*49*), indicating a Mo/heme ratio of 0.92, 0.91, 0.90, 0.81, and 0.88 for G473D, G473A, G473W, G473D/R212A, and A208D, respectively.

Laser Flash Photolysis Studies. Laser flash photolysis experiments were performed anaerobically on 0.50 mL of

Table 1: Oligomeric-State and Steady-State Kinetic Parameters for Wild-Type (wt), G473A, G473W, G473D, and A208D Human SO at pH 8.5 and 6.0[a]

		pH 8.5			pH 6.0		
	oligomeric state	k_{cat} (s^{-1})	$K_m^{sulfite}$ (μM)	$k_{cat}/K_m^{sulfite}$ (M^{-1} s^{-1})	k_{cat} (s^{-1})	$K_m^{sulfite}$ (μM)	$k_{cat}/K_m^{sulfite}$ (M^{-1} s^{-1})
wt	dimer	26.9	8.25	3.26×10^6	13.2	1.29	1.05×10^7
G473A	dimer	28.4	107	2.65×10^5	4.15	4.53	9.2×10^5
G473W	monomer	2.48	2.03×10^3	1.22×10^3	0.60	1910	314
G473D	monomer	0.54	2.04×10^3	265	0.14	1660	84
A208D	dimer	0.75	1.39×10^3	539	0.15	69.2	2168

[a] Solutions contained 20 mM Tris (pH 8.5) or 20 mM Bis-Tris (pH 6.0). The pH was adjusted to 8.5 or 6.0 with acetic acid. G473D/R212A exists in an equilibrium between monomeric and dimeric forms (*56*). The activity of G473D/R212A human SO was undetectable.

solutions containing 5-deazariboflavin (dRF) and 0.5 mM freshly prepared semicarbazide as the sacrificial reductant. The laser apparatus and associated visible absorbance detection system have been extensively described (*52*), as has the basic photochemical process by which 5-deazariboflavin semiquinone (dRFH$^\bullet$) is generated by reaction between triplet-state dRF and the sacrificial reductant and used to reduce redox-active proteins (*53*). Briefly, a N_2 laser [Photochemical Research Associates (PRA), London, ON] was used to pump a dye laser (BBQ 2A368 dye, 396 nm wavelength maximum; PRA), which was focused onto the sample cell, and used to trigger the reactions. The dRF solution was deaerated by vigorously bubbling it with H_2O-saturated O_2-free argon for at least 2 h, and the absorption change at 510 nm due to dRFH$^\bullet$ formation and disappearance was monitored to check the degassing efficiency, prior to addition of microliter volumes of concentrated protein. Argon was purged over the surface of the protein solution to remove traces of O_2 before mixing the protein droplet into the bulk solution. Experiments were performed at room temperature. Further details concerning the photochemical process, which are particularly relevant to the SO proteins, are presented below. Generally, data from 6−12 laser flashes were averaged. Transient absorbance changes at 555 nm were analyzed using SIFIT, obtained from OLIS Inc. (Jefferson, GA).

Steady-State Kinetic Studies. Initial velocities were determined by following the reduction of a freshly prepared oxidized cytochrome *c* (type VI, Sigma-Aldrich Co.) solution at 550 nm, using an extinction coefficient change of 19 630 M^{-1} cm^{-1}. Steady-state kinetic assays were conducted aerobically using a saturating concentration of cytochrome *c* and varying the concentration of sodium sulfite as previously described (*51*). The buffers used were 20 mM Tris [tris(hydroxymethyl)aminomethane, pH 8.5] or 20 mM Bis-Tris [bis(2-hydroxyethyl)aminotris(hydroxymethyl)-methane, pH 6.0], adjusted to the appropriate pH with acetic acid to minimize the possibility of anion inhibition (*51*, *54*).

EPR Studies. EPR samples of G473D, G473A, G473W, G473D/R212A, and A208D human SO were obtained by reducing the protein with a 20-fold molar excess of sodium sulfite in buffers containing 25 mM Pipes (1,4-piperazinediethanesulfonic acid) and 25 mM Bicine [*N*,*N*-bis(2-hydroxyethyl)glycine]. The pH of the buffer was adjusted with NaOH. Buffer exchange into D_2O was accomplished by concentrating the protein samples to 20 μL, and then diluting to 0.5 mL with the appropriate buffer in D_2O. This procedure was repeated three times. The pD value was calculated as described by Glasoe and Long (*55*); i.e., $pD_{true} = pD_{apparent} + 0.4$. CW EPR spectra were recorded at 77 K on an ESP-300E Bruker X-band spectrometer.

RESULTS

Oligomeric-State and Steady-State Kinetics of G473D, G473A, G473W, and A208D Human SO. The oligomeric state, verified by gel filtration and sedimentation equilibrium, and the values of k_{cat}, $K_m^{sulfite}$, and $k_{cat}/K_m^{sulfite}$ of wild-type, G473D, G473A, G473W, and A208D human SO are shown in Table 1. The G473D/R212A mutant exists in an equilibrium between monomeric and dimeric forms, as verified by sedimentation equilibrium studies (*56*).

Steady-state kinetic studies showed a remarkable decrease in $k_{cat}/K_m^{sulfite}$ of 4 orders of magnitude in G473D and A208D human SO mutants, along with 2 order of magnitude changes in the individual parameters k_{cat} and $K_m^{sulfite}$. These results strongly suggest that both enzymatic turnover and the binding of sulfite are substantially inhibited in these two mutants. The kinetic properties of the G473A mutant are much less affected, with an only 10-fold decrease in $k_{cat}/K_m^{sulfite}$ that is entirely due to the K_m value. Note also that the kinetic behavior of G473W is intermediate between that of the wild type and G473D and that the G473D and G473W mutants are monomeric in solution.

Photochemical Reduction of Human SO by Deazariboflavin Semiquinone. The photochemical reduction of the Fe(III) center of the heme moiety of human SO was monitored at 555 nm by laser flash photolysis-induced transient absorbance changes. The flash-induced difference spectra of the G473D, G473A, and A208D human SO mutants exhibited peaks and isosbestic points (data not shown) similar to those obtained with the wild-type human SO (*30*) and native chicken SO (*33*). These difference spectra confirm that the transient absorbance changes observed at 555 nm are directly related to reduction and reoxidation of the *b*-type heme prosthetic group (see below).

Figure 3 shows a typical transient kinetic trace obtained at 555 nm upon laser flash photoexcitation of a solution containing oxidized G473A human SO, 5-deazariboflavin (dRF), and semicarbazide (AH_2). The kinetic behavior can be fully described in terms of eqs 2−5.

$$dRF \xrightarrow{h\nu} {}^1dRF \rightarrow {}^3dRF \quad (2)$$

$${}^3dRF + AH_2 \rightarrow dRFH^\bullet + AH^\bullet \quad (3)$$

$$dRFH^\bullet + Mo(VI)/Fe(III) \rightarrow dRF + Mo(VI)/Fe(II) \quad (4)$$

$$Mo(VI)/Fe(II) \underset{k_r}{\overset{k_f}{\rightleftharpoons}} Mo(V)/Fe(III) \quad (5)$$

The laser pulse produces ^{3}dRF by absorption and intersystem crossing (eq 2), which abstracts a hydrogen atom from

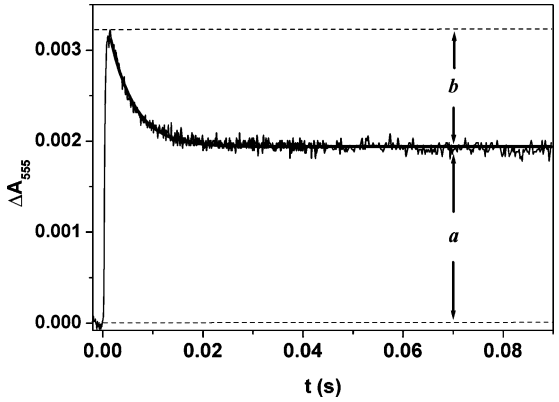

FIGURE 3: Transient obtained at 555 nm upon photoexcitation of a solution containing 8 μM G473A human SO, ~90 μM dRF, 10 mM Tris, and 0.5 mM semicarbazide hydrochloride (pH 7.4). The solid line indicates a single-exponential fit to the IET phase. $K_{eq} = b/a$.

semicarbazide to form the highly reducing dRFH$^{\bullet}$ (eq 3). The initial positive deflection of absorbance from zero in Figure 3 is due to net reduction of the Fe(III) center to the Fe(II) form (eq 4), which has an absorbance maximum at 555 nm. The subsequent slow absorption decay is due to the net IET from Fe(II) to Mo(VI), i.e., the intramolecular reoxidation of Fe(II) (eq 5). The transient does not fall back to the baseline, which clearly indicates the existence of an equilibrium between the Mo(VI)/Fe(II) and Mo(V)/Fe(III) forms of SO (eq 5). The kinetics of this process are independent of G473A SO concentration (data not shown), indicating that the heme reoxidation is an intramolecular process, which is the focus of our interest in this study. The IET rate constants of the G473D and A208D mutants are all independent of protein concentration as well (data not shown), consistent with the intramolecular nature of this electron transfer.

For the case shown in Figure 3, in which the flash-induced reduction of SO (eq 4) occurs much faster than the subsequent IET (eq 5), accurate values for the overall IET rate constant k_{et} ($=k_f + k_r$) and parameters a and b (see Figure 3) can be obtained by fitting the heme reoxidation phase with the exponential function given in eq 6.

$$A_{555} = a + b\exp(-k_{et}t) \tag{6}$$

On the basis of eq 5, parameters a and b in eq 6 have the meanings given in eqs 7 and 8, respectively (where A_0 is the absorbance extrapolated to time zero, assuming that the photochemically induced reduction of SO is instantaneous).

$$a = A_0\frac{k_r}{k_{et}} = A_0\frac{k_r}{k_f + k_r} \tag{7}$$

$$b = A_0\frac{k_f}{k_{et}} = A_0\frac{k_f}{k_f + k_r} \tag{8}$$

$$K_{eq} = \frac{k_f}{k_r} = \frac{b}{a} \tag{9}$$

Thus, the individual IET rate constants k_f and k_r can be calculated from k_{et} and K_{eq} ($=b/a$, eq 9). The IET rate constants and K_{eq} values for wild-type, G473D (transient decay curve shown in Figure 4), G473W, and A208D

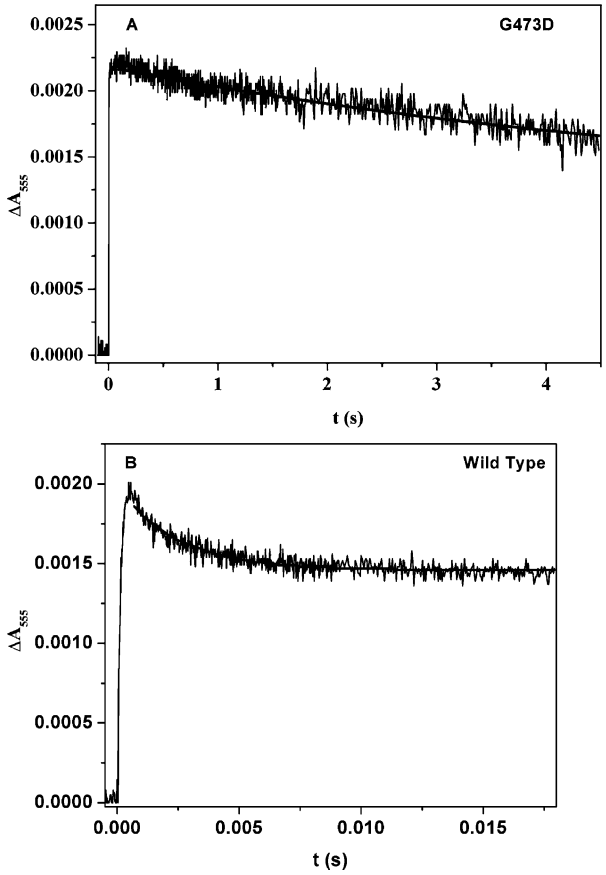

FIGURE 4: Transient obtained at 555 nm upon photoexcitation of a solution containing (A) 8 μM G473D or (B) 9 μM wild-type human SO, with ~90 μM dRF, and 0.5 mM semicarbazide in 20 mM Bis-Tris. The pH was adjusted to 6.0 with acetic acid. The solid line indicates a single-exponential fit to the IET phase.

Table 2: Flash Photolysis Kinetic Parameters for wt, G473D, and A208D Human SO at pH 6.0[a]

	k_{et} (s^{-1})	K_{eq}
wt	411 ± 15	0.36 ± 0.02
G473D	~0.17	ND[b]
ratio (wt/G473D)	~2400	
G473W	~0.11	ND[b]
ratio (wt/G473W)	~ 4000	
A208D	~0.10	ND[b]
ratio (wt/A208D)	~ 4000	

[a] Solutions contained 0.5 mM semicarbazide hydrochloride and 20 mM Bis-Tris. The pH was adjusted to 6.0 with acetic acid. [b] An accurate value of K_{eq} could not be determined because of the unfinished decay within the maximum time range we could use (5 s), beyond which diffusion cannot be excluded.

Table 3: Flash Photolysis Kinetic Parameters for wt and G473A Human SO at pH 7.4[a]

	k_{et} (s^{-1})	K_{eq}
wt	491 ± 11	0.73 ± 0.08
G473A	188 ± 4	0.81 ± 0.03
ratio (wt/G473A)	2.6	1.1

[a] The solutions contained 0.5 mM semicarbazide hydrochloride and 10 mM Tris. The pH was adjusted to 7.4 with hydrochloric acid.

(transient similar to that of G473D, not shown) human SO at pH 6.0 are shown in Table 2. Table 3 shows the values for G473A and wild-type human SO at pH 7.4.

Although we attempted to observe IET in the G473D, G473W, and A208D human SO mutants in the same pH

Table 4: pH Dependence of IET Rate Constants of G473A Human SO[a]

pH	k_{et} (s^{-1})	K_{eq}	k_f (s^{-1})	k_r (s^{-1})
7.09	200 ± 5	1.14 ± 0.32	107 ± 3	93 ± 2
7.42	112 ± 3	1.20 ± 0.18	62 ± 2	50 ± 1
7.53	100 ± 3	1.02 ± 0.15	51 ± 2	49 ± 2
7.71	85 ± 3	1.06 ± 0.06	44 ± 2	41 ± 2
8.00	53 ± 2	0.83 ± 0.07	24 ± 1	29 ± 1

[a] The solutions contained 0.5 mM semicarbazide hydrochloride and 6 mM HCl and were titrated with Tris base so as to achieve the appropriate pH while keeping the Cl^- concentration at ~6.5 mM.

range (approximately 7−8) as for the wild-type enzyme, no decay after heme reduction was observed. For these mutants, the Fe(II) reoxidation phase only began to be detectable at pH 6.0. We presume that this is due to an unfavorable equilibrium above this pH, which may be due to a decrease in the reduction potential of the Mo(VI)/Mo(V) couple. By means of steady-state activity measurements, however, it was observed that the G473D, G473W, and A208D human SO mutants still remained functional at pH 6.0 (k_{cat} = 0.14, 0.60, and 0.15 s^{-1} for G473D, G473W, and A208D, respectively). In addition, the magnitudes of the signal change at 555 nm for heme reduction by deazariboflavin semiquinone in flash photolysis experiments at this pH were comparable to those observed with the wild-type protein at pH 7.4. Under comparable conditions (pH 6.0), the k_{et} values for the G473D, G473W, and A208D mutants are at least 3 orders of magnitude smaller than that for wild-type SO (Table 2; note the remarkable difference in the time scale of the traces for wild-type and G473D SO in Figure 4), whereas the k_{et} value for the G473A mutant is only 2.6-fold smaller than that for the wild type (Table 3). Note also that we were not able to determine a K_{eq} value for the G473D, G473W, and A208D mutants because of the slowness of the decay process (for technical reasons, we are limited to a maximal 5 s time scale in the flash experiment). The K_{eq} value for the G473A mutant is similar to that of wild-type SO (Table 3).

Dependence of IET Rates in G473A on pH. Table 4 shows the values of the IET rate constants for G473A human SO between pH 7.0 and 8.0, in solutions containing low Cl^- concentrations (~6.5 mM). Note that both k_f and k_r for the mutant decrease significantly with an increase in OH^- concentration (Figure 5). Due to the small amplitude and slowness of the signal decay due to IET (see Figure 4A), experiments on G473D and A208D human SO were not conducted over a range of pH values.

EPR of G473D, G473A, G473W, and G473D/R212A Human SO. The EPR parameters for G473D and G473A at low pH (6.2) are given in Table 5. For G473A, addition of 100 mM chloride produces strong coupling from an exchangeable proton, as shown by the CW EPR spectra in H_2O and D_2O buffers (Figure 6), analogous to wild-type human SO under comparable conditions. However, addition of chloride to G473D at pH 6.2 yields a mixture. CW EPR spectra of G473W and G473D/R212A at low pH [25 mM Bicine, 25 mM Pipes, and 100 mM NaCl (pH 6.2)] show a mixture of species (cf. Figures S1 and S2 of the Supporting Information), which is different from the wild-type spectrum under comparable conditions.

The CW EPR spectra of G473D, G473A, G473W, and G473D/R212A at high pH are similar to those of the high-pH form of the wild type (cf. Table 5; Figures S1 and S2 of the Supporting Information).

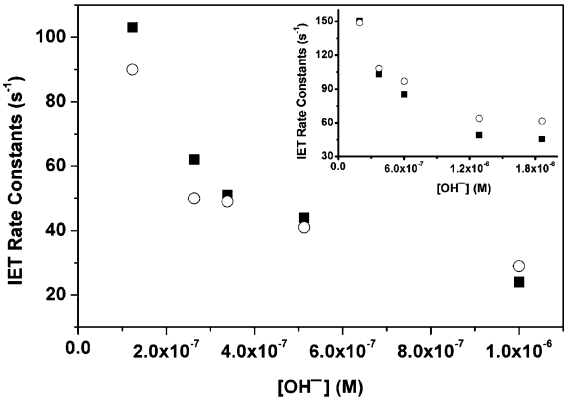

FIGURE 5: Dependence of the rate constants k_f (■) and k_r (○) of G473A human SO on hydroxide ion concentration. Solutions contained 0.5 mM semicarbazide hydrochloride and 6 mM HCl. For all experiments, the Tris base concentration was chosen to achieve the appropriate pH while keeping the Cl^- concentration at ~6.5 mM. The inset is plot of k_f (■) and k_r (○) of wild-type human SO vs hydroxide ion concentration at low Cl^- concentrations (adapted from ref *30*).

Table 5: EPR Parameters of G473D, G473A, G473W, G473D/R212A, and A208D Human SO, and Those of wt Human SO

	g value				A (^{1}H) ($\times 10^{-4}$ cm^{-1})			
	1	2	3	av	1	2	3	av
low pH								
G473D[a]	2.002	1.974	1.965	1.980				
G473A[a]	2.001	1.976	1.965	1.980				
G473A[b]	2.004	1.972	1.967	1.981	7.0	5.7	11.3	8.0
A208D[b]	2.004	1.974	1.968	1.982	9.0	8.0	13.0	10.0
wt[c]	2.004	1.972	1.966	1.981	8.0	7.4	11.9	9.1
high pH								
G473D[d]	1.990	1.966	1.957	1.971				
G473A[e]	1.990	1.967	1.956	1.971				
G473W[e]	1.990	1.966	1.952	1.969				
G473D/R212A[e]	1.990	1.966	1.956	1.971				
A208D[e]	2.004	1.974	1.969	1.982	6.3	5.0	10.7	7.3
wt[f]	1.990	1.966	1.954	1.970				

[a] Buffer of 25 mM Bicine and 25 mM Pipes (pH 6.2). [b] Buffer of 25 mM Bicine, 25 mM Pipes, and 100 mM NaCl (pH 6.2). [c] Buffer of 100 mM Tris and 100 mM NaCl (pH 7.0); cf. ref *25*. [d] Buffer of 25 mM Bicine and 25 mM Pipes (pH 8.6). [e] Buffer of 25 mM Bicine and 25 mM Pipes (pH 9.5). [f] Buffer of 100 mM Bis-Tris propane (pH 9.5); cf. ref *25*.

EPR of A208D Human SO. Figure 7A shows the CW EPR spectrum of A208D at pH 6.2 and pD 5.8 in the presence of 100 mM NaCl, which is similar to the low-pH form of the wild type. Figure 7B shows the CW EPR spectrum of A208D at pH 9.5 and pD 9.1. Note that the EPR spectrum of A208D at pH 9.5 has the same *g* values as the low-pH form of the wild type and shows splitting due to the strong coupling of the nearby exchangeable proton (Figure 7B and Table 5).

DISCUSSION

IET Rates of G473D Human SO. At pH 6.0, the k_{et} value of G473D human SO is only 0.17 s^{-1} (cf. Table 2), which is close to its k_{cat} value at this pH (0.14 s^{-1}). Thus, IET in G473D SO becomes the rate-limiting step during catalytic turnover, similar to the results obtained with R160Q human SO (*35*). These severely compromised IET and catalytic rates may seriously retard efficient catalytic turnover of toxic

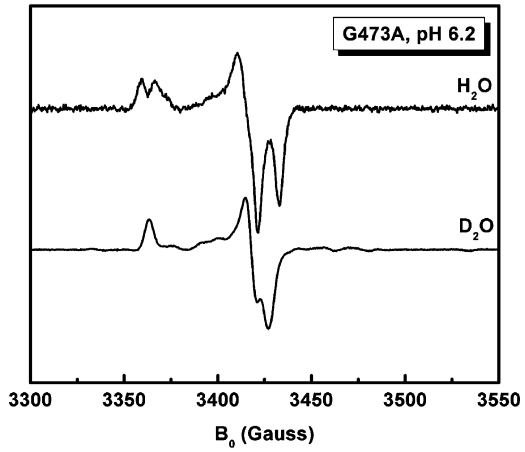

FIGURE 6: CW EPR spectra of G473A human SO obtained at pH 6.2 (top) and pD 5.8 (bottom), in a buffer of 25 mM Bicine, 25 mM Pipes, and 100 mM NaCl.

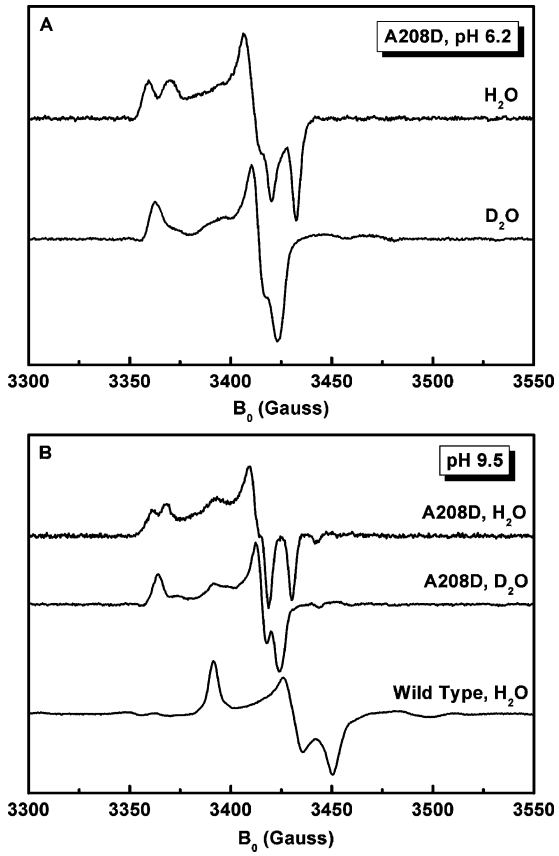

FIGURE 7: (A) CW EPR spectra of A208D human SO at pH 6.2 (top) and pD 5.8 (bottom), in a buffer of 25 mM Bicine, 25 mM Pipes, and 100 mM NaCl. (B) CW EPR spectra of A208D human SO at pH 9.5 (top) and pD 9.1 (middle) and wild-type human SO at pH 9.5 (bottom).

sulfite to sulfate in vivo, thereby helping to explain the fatal effect of the G473D mutation in human SO.

Gel filtration and sedimentation equilibrium studies show that the G473D mutant exists primarily as a monomer in solution (*56*), demonstrating disruption of the interactions that allow dimer formation in the wild-type enzyme. The overall structure of the G473D human SO has also been evaluated by circular dichroism (CD) spectroscopy. We have observed that the far-UV CD spectrum (200−240 nm) of G473D exhibits pronounced differences in shape, intensity, and position of the CD bands from that of the wild-type protein (*56*), which certainly indicate a significant change in backbone conformation. On the basis of these observations, the slow IET in G473D could be a result of a large change in backbone conformation. From the structure of chicken SO, such a conformational change is likely a consequence of the buried nature of G473 (Figure 1), which in the mutant would place a bulky charged residue close to the two hydrophobic residues, M215 and V221. For the G473D mutant, on the basis of thermodynamic considerations alone, the presence of a negative charge in the same environment seems to be highly unfavorable. However, in the absence of a structure for this mutant, we can only speculate about the reasons for the dramatic effects that are seen. One possibility is that the conformational change is due to the fact that G451 in chicken SO (G473 in human SO), with unique torsion angles conferring backbone flexibility, is near P440 (shown in Figure 1), which is in turn probably important in the structural integrity of the C-terminal dimerization domain. Thus, the change in backbone conformation at residue 473 in the human SO mutant could be transmitted to this proline, thereby interfering with dimerization interactions, which could account for the tendency of G473D human SO to exist as a monomer in solution.

Next we consider why the G473D mutation led to impaired IET. We have previously proposed from the viscosity dependence of IET in wild-type human and chicken SO that docking of the heme domain with the Mo domain, possibly driven by electrostatic interactions (*35*), is required for efficient IET (*29*). Very recently, the high-resolution structure of *Starkeya novella* SDH has allowed the identification of contact regions between the Mo and heme domains in a complex in which the cytochrome subunit is in a position for efficient IET (*57*). It is possible that the monomeric nature of the G473D enzyme allows "competition" for docking of the heme domain between the Mo domain and a new exposed site of the dimerization domain. Recently, a comparison of the structures of chicken SO and *A. thaliana* SO makes it possible to identify a region of conserved surface residues in chicken SO that are close to the substrate binding pocket at the entrance of the Mo active site, where its heme domain may transiently dock for efficient IET during enzymatic turnover (*38*). The cartoon of Figure 8 shows the proposed heme docking site with a green arrow (structure I). Motion of the Mo and Fe centers toward each other generates the proposed transient internal complex (structure II) that may facilitate subsequent IET to generate structure III. In the monomeric G473D human SO mutant (structure IV), the exposed dimerization domain may provide access to another heme docking site (red arrow) that competes with the Mo domain site (green arrow), thereby retarding IET.

IET Rates of G473A Human SO. To further understand the dramatic effects of the G473D mutation, the G473A variant was created to test the effect of forcing a change in the torsion angles without the complication of the bulky charged Asp residue at that position. At pH 7.4, the k_{et} and K_{eq} values of G473A human SO are 188 ± 4 s^{-1} and 0.81 ± 0.03, respectively (compared to values for the wild type of 491 ± 11 s^{-1} and 0.73 ± 0.08, respectively; Table 3). Furthermore, the far-UV CD spectra of G473A and wild-type human SO are nearly identical (*56*), indicating the similarity in their secondary structures. In addition, steady-

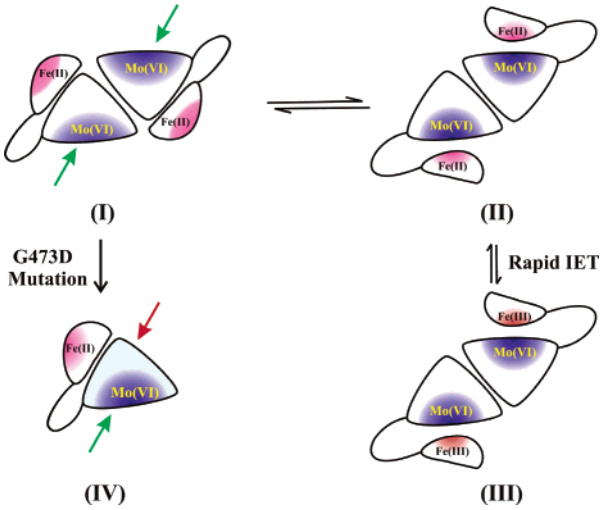

FIGURE 8: Proposed docking of the heme domain to the Mo domain in vertebrate SO that could move the Mo and Fe centers closer together (structure II) than that observed in the crystal structure of dimeric SO (structure I). Subsequently, the transient internal complex (structure II) may facilitate rapid IET to generate structure III. A possible docking site near the Mo domain in the dimeric form is marked with a green arrow. In the monomeric G473D human SO mutant (structure IV), IET may be retarded by competition for docking of the heme domain between the Mo domain site (green arrow) and an alternative docking site on the exposed dimerization domain (red arrow).

state kinetic studies on the G473A mutant showed an only slightly smaller $k_{cat}/K_m^{sulfite}$ value relative to that of the wild type (Table 1), indicating rather similar binding of sulfite. CW EPR spectra of G473A at both low pH (with 100 mM NaCl, Figure 6) and high pH are similar to those of the wild type under the same conditions (Table 5), indicating little or no change in the Mo(V) active site structure. It should also be noted that gel filtration studies showed that the G473A mutant remains a dimer in solution (*56*), similar to the wild type. Together, these results are consistent with the view that in the G473D mutant it is the electrostatic interactions between the negative charge at D473 and its nearby arginines that are responsible for the significant backbone conformational change (see above), and the corresponding much larger decrease in the IET rate constant. In other words, the slow IET and low activity of G473D are not due to a loss of the Gly residue itself. In G473A human SO, at low anion concentrations, both k_f and k_r decrease significantly with an increase in OH^- concentration (Table 4 and Figure 5), which is similar to the pattern observed previously for the wild-type human SO (*30*), again indicating the similarity between G473A and wild-type SO (see above).

IET Rates of G473W and G473D/R212A Human SO. The G473W variant was investigated to study human SO in the monomeric state in the absence of the negative charge contributed by Asp. At pH 6.0, the k_{et} value of the G473W human SO is only $\sim$0.1 s^{-1} (kinetic trace not shown), which is highly impaired relative to that of the wild-type protein. CD data indicate significant backbone change, and sedimentation equilibrium centrifugation and gel filtration studies show that G473W exists primarily as a monomer in solution (*56*). In addition, the CW EPR spectrum of G473W at low pH shows a mixture of species (Figure S1 of the Supporting Information), which is different from the wild-type spectrum under comparable conditions. This is consistent with the CD results.

The introduction of the bulky group (W473) at this position prevents the correct local folding in the dimerization domain, resulting in a monomeric protein with a different conformation. These results clearly demonstrate again that an appropriate conformation is very important for efficient IET and turnover in human SO.

When the G473D mutation is mapped onto the chicken SO crystal structure, it can be seen that the Asp 473 residue would be in steric conflict with Arg 212, preventing the C-terminal domain from folding correctly, thus precluding dimerization. In an attempt to remove the steric conflict of Asp 473 with Arg 212, the double mutant G473D/R212A was generated. Although the double mutant does regain its partial ability to dimerize, there is still significant misfolding at the secondary structure level, as evidenced by CD data (*56*). No IET decay was observed for this mutant. This is not surprising because steady-state kinetics show that the protein is completely inactive. In addition, the CW EPR spectrum of G473D/R212A at low pH shows a mixture of species (Figure S2 of the Supporting Information), which is different from the wild-type spectrum under comparable conditions. These results indicate that the introduction of charged D473 at the buried site disrupts local folding, protein dimerization, and subsequently the overall conformation of the protein, and this impact cannot be offset by nearby substitutions.

IET Rates of A208D Human SO. At pH 6.0, the k_{et} value of A208D human SO is only 0.10 s^{-1} (cf. Table 2), which is close to its k_{cat} value (0.15 s^{-1}). Thus, the severely impaired IET in A208D SO becomes the rate-limiting step during catalytic turnover, and prevents efficient enzymatic turnover, thereby rationalizing the fatal effect of the A208D mutation in human SO.

The slow IET in A208D human SO may also be a result of structural change, although in this case dimerization is not affected. The EPR spectra of A208D (Figure 7 and Table 5) are independent of pH and closely resemble the spectrum of the low-pH form of wild-type human SO. Note that the high-pH form of A208D (Figure 7B) has the *g* values of the low-pH form of the wild type (Table 5), and does show strong couplings due to nearby exchangeable protons. This behavior contrasts with the results for wild-type human SO at high pH, which has distinguishable lower *g* values and shows no proton coupling in the CW EPR (bottom spectrum in Figure 7B). Therefore, the CW EPR data indicate that the A208D mutation perturbs the SO Mo(V) active site structure. In addition, the CD spectrum of A208D (Figure S3 of the Supporting Information) displays some of the same structural perturbations as the monomeric mutant G473D (*56*), even though it is a dimer, which indicates that a structural change in the A208D mutant is at least partially responsible for the IET impairment in this mutant.

In the structure of chicken SO, A186 (A208 in human SO) is buried in the protein (Figure 1). As with the G473D mutation, adding a charged side chain at this buried position is thermodynamically unfavorable. For the Asp residue to remain buried in the hydrophobic core in the A208D variant, the pK_a of the Asp 208 residue may change or the residue may form an ion pair with a nearby Arg residue to remain electrically neutral. The alternative is that the residue may

move to the solvent accessible surface, which would induce a structural change in the protein. Furthermore, on the basis of the structure of chicken SO, adding a charged side chain at residue 186 in chicken SO could interfere with its direct neighbor C185, which is coordinated to the Mo atom (Figure 1), and the nearby Y322, which is part of a hydrophobic pocket formed by I342, L345, V452, and L453. The local structural rearrangements necessary to accommodate this charged residue may affect the substrate binding pocket. To confirm this, the crystal structure of this mutant will have to be determined. However, it is significant that the $k_{cat}/K_m^{sulfite}$ of the A208D mutant does decrease by nearly 6000-fold relative to that of the wild-type enzyme, with a large effect on $K_m^{sulfite}$ (Table 1). The possible changes in the substrate binding pocket may also retard efficient IET by disrupting the proposed interaction between the heme and Mo domains because the conserved docking surface of the Mo domain is close to the substrate binding pocket (see above, Figure 8).

In conclusion, the data presented here provide an experimental explanation for the fatal impact of the G473D and A208D mutations in human SO. The 3 order of magnitude decreases of the rate of IET in G473D and A208D human SO mutants are ascribed to remarkable structural and conformational changes, without affecting the ability of the protein to bind the molybdenum cofactor. Thus, this work demonstrates the importance of the appropriate conformation of human SO in efficient IET and rapid turnover. Steady-state kinetic studies on these mutants (*56*) indicate that the interaction between the heme and molybdenum domains is important for the cyt *c* interaction, although the mutations are not in the heme domain, which is consistent with this work.

This work also suggests the importance of the conserved surface near the Mo site for efficient IET by appropriate docking of the heme domain. This work should inspire new efforts to carry out systematic mutagenesis studies on conserved surface residues in SO enzymes, especially of the strictly conserved charged residues near the Mo center in human SO. Further flash photolysis studies on mutants at these conserved charged surface residues should provide additional insights into the role of surface charge in the docking of the heme domain and IET in SO.

ACKNOWLEDGMENT

We thank Dr. Arnold M. Raitsimring for recording the CW EPR spectra. We thank Sandra Jaramillo-Busquets for assistance in purification of the sulfite oxidase proteins used in this study.

SUPPORTING INFORMATION AVAILABLE

CW EPR spectra of G473D/R212A and G473W human SO mutants and CD spectra of A208D and wild-type human SO. This material is available free of charge via the Internet at http://pubs.acs.org.

REFERENCES

1. Kisker, C. (2001) Sulfite Oxidase, in *Handbook of Metalloproteins* (Messerschmidt, A., Huber, R., Poulos, T., and Wieghardt, K., Eds.) Vol. 2, pp 1121−1135, Wiley, New York.
2. Schindelin, H., Kisker, C., and Rajagopalan, K. V. (2001) Molybdopterin from molybdenum and tungsten enzymes, in *Advances in Protein Chemistry*, Vol. 58, pp 47−94, Academic Press, San Diego.
3. Rajagopalan, K. V., and Johnson, J. L. (2002) Sulfite Oxidase, in *Wiley Encyclopedia of Molecular Medicine* (Creighton, T. E., Ed.) pp 3048−3051, Wiley, New York.
4. Hille, R. (2002) Molybdenum enzymes containing the pyranopterin cofactor: An overview, in *Metal Ions in Biological Systems, Volume 39: Molybdenum and Tungsten: Their Roles in Biological Processes* (Sigel, A., and Sigel, H., Eds.) pp 187−226, Marcel Dekker, New York.
5. Tunney, J. M., McMaster, J., and Garner, C. D. (2004) Molybdenum and tungsten enzymes, in *Comprehensive Coordination Chemistry II* (McClevery, J. A., and Thomas, J. M., Eds.) Vol. 8, pp 459−477, Elsevier Pergamon, New York.
6. Hille, R. (1996) The mononuclear molybdenum enzymes, *Chem. Rev. 96*, 2757−2816.
7. Eilers, T., Schwarz, G., Brinkmann, H., Witt, C., Richter, T., Nieder, J., Koch, B., Hille, R., Hänsch, R., and Mendel, R. R. (2001) Identification and biochemical characterization of *Arabidopsis thaliana* sulfite oxidase: A new player in plant sulfur metabolism, *J. Biol. Chem. 276*, 46989−46994.
8. Kappler, U., Bennett, B., Rethmeier, J., Schwarz, G., Deutzmann, R., McEwan, A. G., and Dahl, C. (2000) Sulfite:cytochrome *c* oxidoreductase from *Thiobacillus novellus*: Purification, characterization, and molecular biology of a heterodimeric member of the sulfite oxidase family, *J. Biol. Chem. 275*, 13202−13212.
9. Campbell, W. H. (1999) Nitrate reductase structure, function and regulation: Bridging the gap between biochemistry and physiology, *Annu. Rev. Plant Physiol. Plant Mol. Biol. 50*, 277−303.
10. Johnson, J. L. (2003) Prenatal diagnosis of molybdenum cofactor deficiency and isolated sulfite oxidase deficiency, *Prenatal Diagn. 23*, 6−8.
11. Johnson, J. L., and Duran, M. (2001) Molybdenum cofactor deficiency and isolated sulfite deficiency, in *The Metabolic and Molecular Bases of Inherited Disease* (Scriver, C., Beaudet, A., Sly, W., and Valle, D., Eds.) 8th ed., pp 3163−3177, McGraw-Hill, New York.
12. Dublin, A. B., Hald, J. K., and Wootton-Gorges, S. L. (2002) Isolated sulfite oxidase deficiency: MR imaging features, *Am. J. Neuroradiol. 23*, 484−485.
13. Matthies, A., Rajagopalan, K. V., Mendel, R. R., and Leimkuhler, S. (2004) Evidence for the physiological role of a rhodanese-like protein for the biosynthesis of the molybdenum cofactor in humans, *Proc. Natl. Acad. Sci. U.S.A. 101*, 5946−5951.
14. Schwarz, G., Santamaria-Araujo, J. A., Wolf, S., Lee, H. J., Adham, I. M., Gröne, H. J., Schwegler, H., Sass, J. O., Otte, T., Hänzelmann, P., Mendel, R. R., Engel, W., and Reiss, J. (2004) Rescue of lethal molybdenum cofactor deficiency by a biosynthetic precursor from *Escherichia coli*, *Hum. Mol. Genet. 13*, 1249−1255.
15. Johnson, J. L., Coyne, K. E., Garrett, R. M., Zabot, M.-T., Dorche, C., Kisker, C., and Rajagopalan, K. V. (2002) Isolated sulfite oxidase deficiency: Identification of 12 novel SUOX mutations in 10 patients, *Hum. Mutat. 20*, 74.
16. Johnson, J. L., Rajagopalan, K. V., Renier, W. O., Van der Burgt, I., and Ruitenbeek, W. (2002) Isolated sulfite oxidase deficiency: Mutation analysis and DNA-based prenatal diagnosis, *Prenatal Diagn. 22*, 433−436.
17. Lee, H. F., Mak, B. S. C., Chi, C. S., Tsai, C. R., Chen, C. H., and Shu, S. G. (2002) A novel mutation in neonatal isolated sulphite oxidase deficiency, *Neuropediatrics 33*, 174−179.
18. Lam, C. W., Li, C. K., Lai, C. K., Tong, S. F., Chan, K. Y., Ng, G. S. F., Yuen, Y. P., Cheng, A. W. F., and Chan, Y. W. (2002) DNA-based diagnosis of isolated sulfite oxidase deficiency by denaturing high-performance liquid chromatography, *Mol. Genet. Metab. 75*, 91−95.
19. Garrett, R. M., Johnson, J. L., Graf, T. N., Feigenbaum, A., and Rajagopalan, K. V. (1998) Human sulfite oxidase R160Q: Identification of the mutation in a sulfite oxidase-deficient patient and expression and characterization of the mutant enzyme, *Proc. Natl. Acad. Sci. U.S.A. 95*, 6394−6398.
20. Kisker, C., Schindelin, H., Pacheco, A., Wehbi, W., Garrett, R. M., Rajagopalan, K. V., Enemark, J. H., and Rees, D. C. (1997) Molecular basis of sulfite oxidase deficiency from the structure of sulfite oxidase, *Cell 91*, 973−983.
21. Rajagopalan, K. V. (1980) Sulphite oxidase, in *Molybdenum and Molybdenum-Containing Enzymes* (Coughlan, M. P., Ed.) pp 241−272, Pergamon Press, Oxford, U.K.

22. Enemark, J. H., and Cosper, M. M. (2002) Molybdenum enzymes and sulfur metabolism, in *Metal Ions in Biological Systems, Volume 39: Molybdenum and Tungsten: Their Roles in Biological Processes* (Sigel, A., and Sigel, H., Eds.) pp 621−654, Marcel Dekker, New York.
23. Enemark, J. H., Astashkin, A. V., and Raitsimring, A. M. (2003) Variable frequency pulsed EPR studies of molybdenum enzymes: Structure of molybdenum enzymes, in *Paramagnetic Resonance of Metallobiomolecules* (Telser, J. A., Ed.) ACS Symposium Series 858, pp 179−192, American Chemical Society, Washington, DC.
24. Astashkin, A. V., Raitsimring, A. M., Feng, C., Johnson, J. L., Rajagopalan, K. V., and Enemark, J. H. (2002) Pulsed EPR studies of nonexchangeable protons near the Mo(V) center of sulfite oxidase: Direct detection of the α-proton of the coordinated cysteinyl residue and structural implications for the active site, *J. Am. Chem. Soc. 124*, 6109−6118.
25. Astashkin, A. V., Mader, M. L., Pacheco, A., Enemark, J. H., and Raitsimring, A. M. (2000) Direct detection of the proton-containing group coordinated to Mo(V) in the high pH form of chicken liver sulfite oxidase by refocused primary ESEEM spectroscopy: Structural and mechanistic implications, *J. Am. Chem. Soc. 122*, 5294−5302.
26. Raitsimring, A. M., Pacheco, A., and Enemark, J. H. (1998) ESEEM investigations of the high pH and low pH forms of chicken liver sulfite oxidase, *J. Am. Chem. Soc. 120*, 11263−11278.
27. Pacheco, A., Basu, P., Borbat, P., Raitsimring, A. M., and Enemark, J. H. (1996) Multifrequency ESEEM spectroscopy of sulfite oxidase in phosphate buffer: Direct evidence for coordinated phosphate, *Inorg. Chem. 35*, 7001−7008.
28. Ferapontova, E. E., Ruzgas, T., and Gorton, L. (2003) Direct electron transfer of heme- and molybdopterin cofactor-containing chicken liver sulfite oxidase on alkanethiol-modified gold electrodes, *Anal. Chem. 75*, 4841−4850.
29. Feng, C., Kedia, R. V., Hazzard, J. T., Hurley, J. K., Tollin, G., and Enemark, J. H. (2002) Effect of solution viscosity on intramolecular electron transfer in sulfite oxidase, *Biochemistry 41*, 5816−5821.
30. Feng, C., Wilson, H. L., Hurley, J. K., Hazzard, J. T., Tollin, G., Rajagopalan, K. V., and Enemark, J. H. (2003) Role of conserved tyrosine 343 in intramolecular electron transfer in human sulfite oxidase, *J. Biol. Chem. 278*, 2913−2920.
31. Pacheco, A., Hazzard, J. T., Tollin, G., and Enemark, J. H. (1999) The pH dependence of intramolecular electron transfer rates in sulfite oxidase at high and low anion concentrations, *J. Biol. Inorg. Chem. 4*, 390−401.
32. Sullivan, E. P., Jr., Hazzard, J. T., Tollin, G., and Enemark, J. H. (1992) Inhibitions of intramolecular electron transfer in sulfite oxidase by anion binding, *J. Am. Chem. Soc. 114*, 9662−9663.
33. Sullivan, E. P., Jr., Hazzard, J. T., Tollin, G., and Enemark, J. H. (1993) Electron transfer in sulfite oxidase: Effects of pH and anions on transient kinetics, *Biochemistry 32*, 12465−12470.
34. Page, C. C., Moser, C. C., Chen, X., and Dutton, P. L. (1999) Natural engineering principles of electron tunnelling in biological oxidation−reduction, *Nature 402*, 47−52.
35. Feng, C., Wilson, H. L., Hurley, J. K., Hazzard, J. T., Tollin, G., Rajagopalan, K. V., and Enemark, J. H. (2003) Essential role of conserved arginine 160 in intramolecular electron transfer in human sulfite oxidase, *Biochemistry 42*, 12235−12242.
36. Elliott, S. J., McElhaney, A. E., Feng, C., Enemark, J. H., and Armstrong, F. A. (2002) A voltammetric study of interdomain electron transfer within sulfite oxidase, *J. Am. Chem. Soc. 124*, 11612−11613.
37. Codd, R., Astashkin, A. V., Pacheco, A., Raitsimring, A. M., and Enemark, J. H. (2002) Pulsed ELDOR spectroscopy of the Mo(V)/Fe(III) state of sulfite oxidase prepared by one-electron reduction with Ti(III) citrate, *J. Biol. Inorg. Chem. 7*, 338−350.
38. Schrader, N., Fischer, K., Theis, K., Mendel, R. R., Schwarz, G., and Kisker, C. (2003) The crystal structure of plant sulfite oxidase provides insights into sulfite oxidation in plants and animals, *Structure 11*, 1251−1263.
39. Liang, Z. X., Kurnikov, I. V., Nocek, J. M., Mauk, A. G., Beratan, D. N., and Hoffman, B. M. (2004) Dynamic docking and electron transfer between Zn-myoglobin and cytochrome b_5, *J. Am. Chem. Soc. 126*, 2785−2798.
40. Liu, L., Hong, J., and Ogawa, M. Y. (2004) Gated electron transfer as a probe of the configurational dynamics of peptide−protein complexes, *J. Am. Chem. Soc. 126*, 50−51.
41. Ren, Y., Wang, W. H., Wang, Y. H., Case, M., Qian, W., McLendon, G., and Huang, Z. X. (2004) Mapping the electron-transfer interface between cytochrome b_5 and cytochrome *c*, *Biochemistry 43*, 3527−3536.
42. Leys, D., Basran, J., Talfournier, F., Sutcliffe, M. J., and Scrutton, N. S. (2003) Extensive conformational sampling in a ternary electron-transfer complex, *Nat. Struct. Biol. 10*, 219−225.
43. Jeuken, L. J. C. (2003) Conformational reorganisation in interfacial protein electron transfer, *Biochim. Biophys. Acta 1604*, 67−76.
44. Hurley, J. K., Morales, R., Martinez-Julvez, M., Brodie, T. B., Medina, M., Gomez-Moreno, C., and Tollin, G. (2002) Structure−function relationships in *Anabaena* ferredoxin/ferredoxin:NADP$^+$ reductase electron transfer: Insights from site-directed mutagenesis, transient absorption spectroscopy and X-ray crystallography, *Biochim. Biophys. Acta 1554*, 5−21.
45. Aguey-Zinsou, K.-F., Bernhardt, P. V., Kappler, U., and McEwan, A. G. (2003) Direct electrochemistry of a bacterial sulfite dehydrogenase, *J. Am. Chem. Soc. 125*, 530−535.
46. Feng, C., Kappler, U., Tollin, G., and Enemark, J. H. (2003) Intramolecular electron transfer in a bacterial sulfite dehydrogenase, *J. Am. Chem. Soc. 125*, 14696−14697.
47. Leimkuhler, S., and Rajagopalan, K. V. (2001) In vitro incorporation of nascent molybdenum cofactor into human sulfite oxidase, *J. Biol. Chem. 276*, 1837−1844.
48. Temple, C. A., Tyler, N. G., and Rajagopalan, K. V. (2000) Optimization of expression of human sulfite oxidase and its molybdenum domain, *Arch. Biochem. Biophys. 383*, 281−287.
49. Garrett, R. M., and Rajagopalan, K. V. (1996) Site-directed mutagenesis of recombinant sulfite oxidase: Identification of cysteine 207 as a ligand of molybdenum, *J. Biol. Chem. 271*, 7387−7391.
50. Garrett, R. M., and Rajagopalan, K. V. (1994) Molecular cloning of rat liver sulfite oxidase-expression of a eukaryotic Mo-pterin-containing enzyme in *Escherichia coli*, *J. Biol. Chem. 269*, 272−276.
51. Wilson, H. L., and Rajagopalan, K. V. (2004) The role of tyrosine 343 in substrate binding and catalysis by human sulfite oxidase, *J. Biol. Chem. 279*, 15105−15113.
52. Hurley, J. K., Weber-Main, A. M., Stankovich, M. T., Benning, M. M., Thoden, J. B., Vanhooke, J. L., Holden, H. M., Chae, Y. K., Xia, B., Cheng, H., Markley, J. L., Martínez-Júlvez, M., Gómez-Moreno, C., Schmeits, J. L., and Tollin, G. (1997) Structure−function relationships in *Anabaena* ferredoxin: Correlations between X-ray crystal structures, reduction potentials, and rate constants of electron transfer to ferredoxin:NADP$^+$ reductase for site-specific ferredoxin mutants, *Biochemistry 36*, 11100−11117.
53. Tollin, G. (2001) Interprotein and intraprotein electron transfer mechanisms, in *Electron Transfer in Chemistry* (Balzani, V., Ed.) Vol. IV, pp 202−231, Wiley-VCH, Weinheim, Germany.
54. Brody, M. S., and Hille, R. (1999) The kinetic behavior of chicken liver sulfite oxidase, *Biochemistry 38*, 6668−6677.
55. Glasoe, P. K., and Long, F. A. (1960) Use of glass electrodes to measure acidities in deuterium oxide, *J. Phys. Chem. 64*, 188−190.
56. Wilson, H. L., Wilkinson, S. R., and Rajagopalan, K. V. (2005) *Biochemistry* (submitted for publication).
57. Kappler, U., and Bailey, S. (2005) Molecular basis of intramolecular electron transfer in sulfite-oxidizing enzymes is revealed by high-resolution structure of a heterodimeric complex of the catalytic molybdopterin subunit and a *c*-type cytochrome subunit, *J. Biol. Chem. 280*, 24999−25007.

BI050907F